Dynamics of rumor propagation on small-world networks

Damián H. Zanette

*Consejo Nacional de Investigaciones Científicas y Técnicas, Centro Atómico Bariloche and Instituto Balseiro, 8400 Bariloche,
Río Negro, Argentina*

We study the dynamics of an epidemiclike model for the spread of a rumor on a small-world network. It has been shown that this model exhibits a transition between regimes of localization and propagation at a finite value of the network randomness. Here, by numerical means, we perform a quantitative characterization of the evolution in the two regimes. The variant of dynamic small worlds, where the quenched disorder of small-world networks is replaced by randomly changing connections between individuals, is also analyzed in detail and compared with a mean-field approximation.

I. INTRODUCTION

The networks that underlie real social interactions, whose nodes represent single individuals and whose links connect individuals that are expected to interact, vary with time and strongly depend on the kind of interactions involved. Generally, however, social networks exhibit two specific topological properties that are closely related to the nature of social interactions. First, they are highly clustered, which means that two randomly chosen neighbors of a given individual have a relatively large probability of being in turn mutual neighbors. Second, the distance between any two nodes in the network, measured as the number of links of the minimal path connecting the two nodes, is on the average very small as compared with the total number of nodes or links. This is the so-called small-world effect. Small-world networks (SWNs) constitute a mathematical model for social networks that captures these two properties [1]. They are partially disordered networks, interpolating between regular lattices and fully random graphs. In fact, N-node regular lattices with connections beyond nearest neighbors have high clustering, but the average distance between nodes is of order N. On the other hand, the average distance in random networks is of order $\ln N \ll N$, but the probability that two neighbors of a given node are mutual neighbors is of order N^{-1}. For moderate disorder, SWNs preserve the two desirable properties of ordered and random networks [2–5], and are, therefore, a convenient tool for the mathematical study of social processes [6].

Small-world networks are built starting from an ordered lattice with moderately high connectivity, which insures high clustering. Then, each link is removed with probability p and reconnected between two randomly selected nodes. This process creates a shortcut between two otherwise distant regions of the network. The probability p measures the degree of disorder or *randomness* of the resulting graph. For $p=0$ order is fully preserved, while for $p=1$ a random graph is obtained. Note, however, that the average connectivity is constant.

Topological properties of SWNs, such as the average distance between nodes, display a crossover from the behavior observed in regular lattices to that of random graphs at a randomness $p \sim N^{-1}$. In the limit of an infinitely large network, a critical transition between both regimes occurs at $p_c=0$ [7,8]. Similar transitions at the same critical point are found for some simple dynamical processes on SWNs, such as for Ising-like spin systems [5] and ensembles of coupled oscillators. In contrast, it has been recently shown that other kinds of processes display a transition between qualitatively different dynamical regimes at finite values of the randomness. Specifically, in an epidemiological model where an initially susceptible individual infected by contagion undergoes a disease cycle that returns to the susceptible state, a transition at finite p occurs between a regime where the disease cycles of different individuals are temporally uncorrected (low p) to a regime where the cycles synchronize (high p) [9]. Moreover, in an epidemiclike model for rumor propagation a quantitatively similar transition has been found between a regime where the rumor remains localized (low p) to a regime where it spreads over a finite fraction of the network (high p) [10].

The critical-phenomenon nature of the transition found in the model of rumor propagation has been convincingly proven by means of finite-size scaling analysis [10]. This paper, on the other hand, focuses on a detailed characterization of the dynamical properties of the same model, with emphasis on the effects introduced by the small-world topology. In the following section we introduce the model and summarize the main results on the critical transition between the regimes of localization and propagation. The core of the paper, Secs. III and IV, is devoted to establishing the connection between the several parameters of our model and suitable quantities that characterize its evolution. This is done both in quenched small-world networks and in the so-called dynamic small worlds, where quenched disorder in the interaction links is replaced by stochastic choice of the interaction partners. We emphasize similarities and differences between both cases. Finally, we summarize and discuss the main results.

II. MODEL OF RUMOR PROPAGATION

Consider a population formed by N individuals where, at each time step, each individual adopts one of three possible states. In the first state, the individual has not heard the rumor yet. In the second state, the individual is aware of the

rumor and is willing to transmit it. Finally, in the third state, the individual has heard the rumor but has lost the interest in it, and does not transmit it. By analogy with SIR (susceptible-infected-refractory) epidemiological models [11], these three states are, respectively, called susceptible, infected, and refractory. At the beginning, only one individual is infected and all the remnant population is susceptible. The dynamical rules act as follows [12]. At each time step, an individual i is chosen at random from the infected population. This individual contacts one of her neighbors, say j. If j is in the susceptible state, i transmits the rumor and j becomes infected. If, on the other hand, j is already infected or refractory, then i loses her interest in the rumor and becomes refractory.

In qualitative terms, the dynamics can be summarized as follows. In the first stage of the evolution, the number of infected individuals increases and, at a lower rate, the refractory population grows as well. As a consequence, the contacts of infected individuals between themselves and with refractory individuals become more frequent. Eventually, the infected population begins to decline and vanishes, and the evolution stops. At the end, the population is divided into a group of N_R refractory individuals, who have been infected at some stage during the evolution, and a group of susceptible individuals who have never heard the rumor. It has been shown [13] that, in the case where contacts can be established between any two individuals in the population, the fraction $r = \langle N_R \rangle / N$ of refractory individuals at the end of the evolution—averaged over a large number of realizations of the system—approaches a well-defined limit r^* for asymptotically large systems, $N \rightarrow \infty$. This fraction is given by the nontrivial solution to the transcendental equation

$$r^* = 1 - \exp(-2r^*), \tag{1}$$

i.e., $r^* \approx 0.796$. In other words, some 20% of the population never becomes aware of the rumor.

We are here interested in the case where contacts between individuals are established along the links imposed by a socially plausible structure, namely, a small-world network. As advanced in the Introduction, SWNs are built starting from an ordered lattice, with one individual at each node. We choose a one-dimensional array with periodic boundary conditions, where each node is connected to its $2K$ nearest neighbors, i.e., to the K nearest neighbors clockwise and counterclockwise. Then each of the K clockwise connections of each node i is rewired with probability p to a randomly chosen node j, not belonging to the neighborhood of i. A shortcut is thus created. We avoid double and multiple links between node, and discard realizations where the SWN becomes disconnected.

Previous analysis of this system, focused on the characterization of its final state, has revealed that a critical transition between two well-differentiated regimes occurs at a finite value p_c of the randomness [10]. For $p < p_c$, the final number N_R of refractory individuals, when averaged over many realizations of the system, is independent of the population size. Therefore, as $N \rightarrow \infty$, the ratio $r = \langle N_R \rangle / N$ tends to vanish. In such limit, only an infinitesimal fraction of the
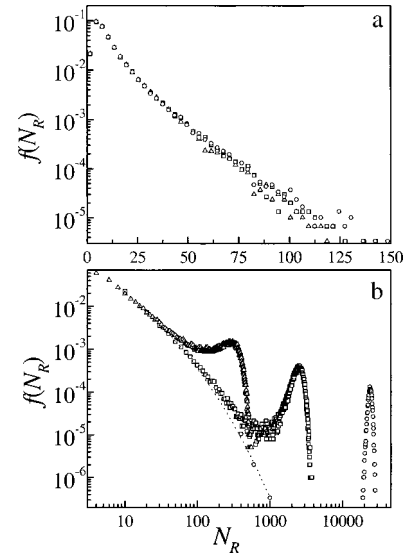

FIG. 1. Normalized frequency distribution $f(N_R)$ of the number of refractory individuals at the end of the evolution, N_R, for $K = 2$ and two values of the small-world randomness, (a) $p = 0.05$ and (b) $p = 0.3$. Different symbols correspond to $N = 10^3$ (triangles), $N = 10^4$ (squares), and $N = 10^5$ (circles). Frequency counts were obtained from series of 10^5 realizations for each parameter set.

population becomes aware of the rumor, which remains localized in a small neighborhood of its origin. On the other hand, for $p > p_c$ the average value of r approaches a constant as N grows. Finite-size scaling analysis in the specific case of $K = 2$ shows that, for asymptotically large systems,

$$r \sim |p - p_c|^\gamma, \tag{2}$$

with $p_c \approx 0.19$ and $\gamma \approx 2.2$. For larger values of K, the critical randomness p_c decreases. The exponent γ, in contrast, seems to be universal.

A clue to the origin of the localization-propagation transition is provided by the distribution $f(N_R)$ of values of N_R over large series of realizations of our system for fixed K, p, and N. Figure 1 shows those distributions for $K = 2$, two values of p—below and above the transition—and three values of N. At each realization, the SWN is constructed anew, and the initially infected individual is randomly chosen from the whole population. For $p < p_c$ the distribution is approximately exponential, and does not depend on N. Consequently, the average value $\langle N_R \rangle$ is also independent of the system size and, as advanced above, the ratio $r = \langle N_R \rangle / N$ decreases as N grows. More specifically, $r \sim N^{-1}$ for large N. In a typical realization for $p < p_c$ the rumor remains localized due to the high interconnectivity of the network at the local level and the scarce density of shortcuts. Transmission occurs between a small group of individuals that rapidly lose their interest in the rumor, and propagation to distant regions is highly improbable.

In contrast, the distribution for $p > p_c$ is bimodal, with two maxima separated by a local minimum. The small-N_R regime is still independent of N and attains a maximum near $N_R = 0$. On the other hand, for large values of N_R, we find an additional bumplike structure, which changes with the sys-

tem size. Specifically, the position of its maximum $N_R^{\max}$ shifts rightward as N grows, as $N_R^{\max} \approx 0.25N$. Since, meanwhile, the area under the bump remains almost constant, this additional structure produces a contribution of order N to the average value $\langle N_R \rangle$. Consequently, r is finite above the transition. While in a realization belonging to the small-N_R regime the rumor remains localized as in the case of $p < p_c$, a typical realization contributing to the bump includes propagation through several shortcuts, thus attaining distant regions in the system.

For $p \approx p_c$, the distribution (not shown in Fig. 1) exhibits power-law dependence for moderate values of N_R, $f(N_R) \sim N_R^{-\alpha}$ with $\alpha \approx 1.5$. The power-law regime terminates at a smooth cutoff, whose position shifts to the right as the system size increases, approximately as $N^{0.5}$ [10].

The localization-propagation transition of our model has been described in terms of static features, namely, the final refractory population N_R, measured when all the interaction events have ceased. In the following section, we focus on our central interest here and study the dynamics of the propagation process.

III. EVOLUTION OF THE INFECTED POPULATION

A complete characterization of the propagation process in our model is given by the evolution of the infected population. Initially, all the population is susceptible, except for an infected individual. Then, at each evolution step, either the number of infected individuals n_I increases to $n_I + 1$ at the expense of the susceptible population, or n_I decreases to $n_I - 1$ and the refractory population grows accordingly. Therefore, the evolution of the number of both susceptible and refractory individuals is implicit in the evolution of n_I. In order to give n_I as a function of time, it must be taken into account that the number of infected individuals varies and, consequently, the real-time duration δt of an evolution step changes. Since at each step an infected individual is chosen at random, δt must be proportional to the probability of choosing that individual, i.e., to the frequency of such event, $\delta t \propto n_I^{-1}$. Therefore, time is to be updated according to

$$t \rightarrow t + \frac{t_0}{n_I(t)}, \qquad (3)$$

where the constant t_0 fixes time units. We choose $t_0 = 1$, so that the unit of time can be associated with the typical time needed by a single infected individual to establish a contact with one of her neighbors.

Figure 2 shows the evolution of the number of infected individuals as a function of time for two single realizations with $N = 10^5$ and $K = 2$, for two values of the network randomness, $p = 0.05$ and 0.3. For $p = 0.05$ the final number of refractory individuals is $N_R = 32$, while for $p = 0.3$ we have $N_R = 22,258$. This latter realization belongs to the large-N_R bump structure in $f(N_R)$ for the corresponding value of p. Realizations for the same randomness but in the small-N_R region are qualitatively similar to that shown in Fig. 2(a).

The graph of n_I as a function of time for small p—or, for $p > p_c$, in the region of small N_R—is reminiscent of a ran-
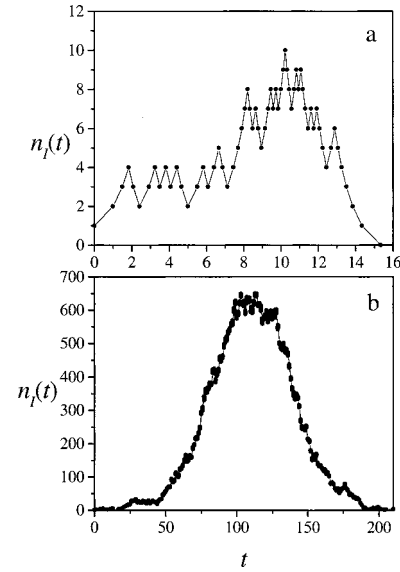

FIG. 2. Evolution of the number $n_I(t)$ of infected individuals as a function of time in two single realizations on a 10^5-node small-world network with $K = 2$, for (a) $p = 0.05$ and (b) $p = 0.3$.

dom walk. As a matter of fact, the evolution of the number of infected individuals can be thought of as a one-dimensional random walk in the n_I space, starting at $n_I = 1$ and with an absorbing boundary condition at the origin, $n_I = 0$, where the evolution terminates. Equivalently, we may think of a first-passage-time problem, with respect to the origin, for a random walker starting at $n_I = 1$ [14]. This analogy, however, is difficult to exploit, since in our case the random walk would be biased by a complex time-dependent asymmetry. In fact, the probability for n_I to grow or decrease depends not only on n_I itself, but also on the number of both susceptible and refractory individuals. The effect of this bias would be particularly strong for the large-N_R realizations with $p > p_c$. In this case, indeed, the evolution of $n_I(t)$ does not resemble a random trajectory but mimics deterministic dynamics affected by a moderate level of noise [see Fig. 2(b)].

The first-passage-time analogy suggests anyway that a compact quantitative characterization of the propagation process is given by the total time T elapsed up to the extinction of the infected population, and the maximum number of infected individuals during the evolution, N_I. In the associated random walk, these two quantities correspond to the first-passage time and the maximum span from the origin, respectively. In order to compare with our previous results, we measure T and N_I as a function of the final refractory population N_R. Note that N_R is directly related to the duration of the propagation process measured in evolution steps. In fact, since the final number of infected individuals is zero, each step where a susceptible individual becomes infected must be compensated by a step where an infected individual becomes refractory. Since an extra step of this latter kind is needed for the first infected individual, the total number of steps necessary for the extinction of the infected population is exactly $2N_R - 1$. On the other hand, due to the changing duration of steps in real time, Eq. (3), the connection between T and N_R is more complex.
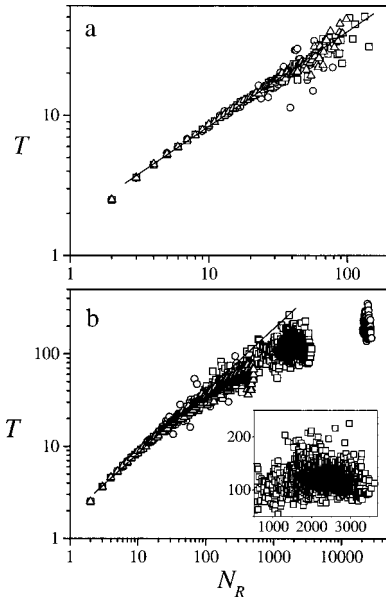
FIG. 3. Total time T up to the extinction of the infected population, as a function of the final number of refractory individuals N_R, for networks with $K=2$ and $N=10^3$ (triangles), 10^4 (squares), and 10^5 (circles). The randomness is (a) $p=0.05$ and (b) $p=0.3$. Both T and N_R were measured in 10^4 realizations for each value of p. In the cases where several values of T were obtained for the same value of N_R, they were averaged. The straight lines have a slope of 2/3. The inset in (b) shows a close-up of the "cloud" at large values of N_R for $N=10^4$, in linear scales.

In Fig. 3, we present measurements of the total time T as a function of N_R over series of 10^4 realizations, for SWNs with $K=2$ and three different sizes, and for two values of the randomness p. For small p there is a quite well-defined power-law dependence, $T \sim N_R^\tau$, spanning almost two orders of magnitude in N_R. Linear fitting of these data yields an exponent τ close to 2/3. This result differs from the value predicted by the random-walk analogy for an unbiased random walk in the n_I space, which gives $\tau=1/2$. On the other hand, it can satisfactorily be reproduced by a random walk with constant bias, with probabilities $P=0.6$ of moving towards $+\infty$ and $1-P=0.4$ of moving in the opposite direction. We recall, however, that the analogy would be strict for a time-dependent bias only. For $p>p_c$ the above power-law dependence is still observed in the small-N_R regime, but apparent deviations appears as N_R grows. In particular, the detached "cloud" of dots observed for $N=10^4$ and 10^5 at large values of N_R—which correspond to realizations in the bump structure observed in $f(N_R)$ (see Fig. 1)—does not satisfy the power-law relation. The total evolution times associated with such realizations are considerably below those predicted by an extrapolation from the small-N_R region, and the difference becomes larger as the size N grows. Note moreover, from the inset in Fig. 3(b), that inside the "cloud" there is no obvious correlation between T and N_R, in contrast with the small-N_R regime. These features make it evident that a qualitative change in the dynamical behavior occurs between the regimes of small and large N_R, as illustrated in Fig. 2.

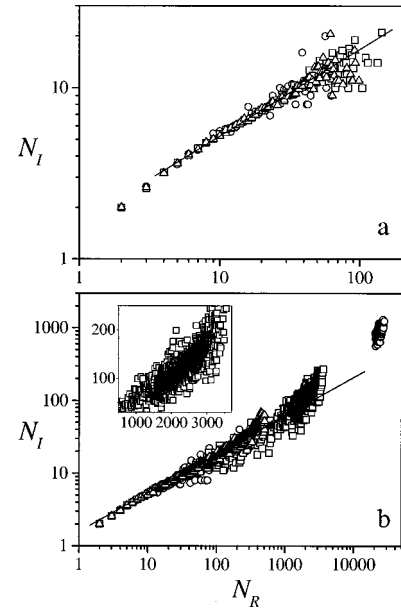Essentially the same features are found for the depen-

FIG. 4. Maximum number of infected individuals during the evolution, N_I, as a function of the final number of refractory individuals, N_R, for networks with $K=2$ and $N=10^3$ (triangles), 10^4 (squares), and 10^5 (circles). The randomness is (a) $p=0.05$ and (b) $p=0.3$. Data were obtained from the same numerical realizations as those of Fig. 3. The straight lines have a slope of 1/2. The inset in (b) shows a close-up of the "cloud" at large values of N_R for $N=10^4$, in linear scale.

dence of the maximum number of infected individuals during the whole evolution, N_I, on N_R, shown in Fig. 4. Now, however, the exponent in the power-law relation $N_I \sim N_R^\nu$, observed to hold in the small-N_R regime, is close to 1/2, which does coincide with the result for an ordinary unbiased random walk. For large N_R, the "clouds" of dots quoted above deviate in this case to higher values of N_I. A detail of the "cloud" for $N=10^5$, shown in the inset of Fig. 4(b), reveals a remnant correlation between N_I and N_R.

Note that the power-law dependence of T and N_I on N_R, implies the relation $T \sim N_I^\mu$, with $\mu=\tau/\nu \approx 1/3$. This relation is expected to hold for small randomness or, more generally, for small N_R.

Through the study of the evolution of the infected population, we have so far examined the dynamical properties of our model for just two values of the small-world randomness p, below and above the localization-propagation transition at p_c. It is now worthwhile to discuss how the results change as p is varied. For $0<p<p_c$, as a matter of fact, the power-law dependence of T and N_I on N_R is not modified. The exponents τ and ν are the same within our numerical precision. On the contrary, above the transition, substantial changes affect the frequency distribution of the final refractory population N_R and its relation to T and N_I.

In the first place, the relative number of realizations in the small-N_R regime and in the bump at large N_R varies considerably with p. Figure 5 shows the fraction ρ of realizations in the large-N_R bump as a function of p for three values of N and $K=2$. This fraction grows from $\rho \approx 0.35$ for $p=0.3$ to $\rho \approx 0.7$ for the maximum randomness $p=1$. As expected,
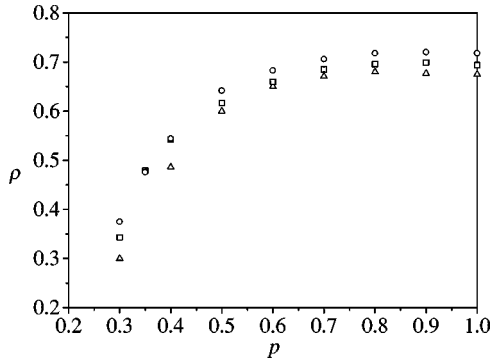
FIG. 5. Fraction ρ of realizations in the bump at large N_R as a function of the small-world randomness p, for networks with $K = 2$ and $N = 10^3$ (triangles), 10^4 (squares), and 10^5 (circles). Data obtained from series of 10^3 realizations for each value of p.

realizations where the rumor attains a significant fraction of the population become more frequent as the network randomness grows. Note moreover that the dependence with the system size N is quite weak, but there is no clear indication of saturation for large N.

As for the dependence of the total evolution time T and the maximum number of infected individuals N_I on the final refractory population N_R, the small-N_R regime exhibits no significant modifications as p changes. The power-law dependence with the same exponents is maintained, as expected from the fact that the realizations in this regime correspond to propagation of the rumor over a limited neighborhood of its origin. In contrast, the bump in $f(N_R)$ varies in position and the corresponding values of T and N_I change. In Fig. 6, we show the average values of T and N_I as a function of the fraction $r = \langle N_R \rangle / N$ corresponding to realizations in the bump for several values of p. Roughly speaking, each dot represents the centers of the "clouds" referred
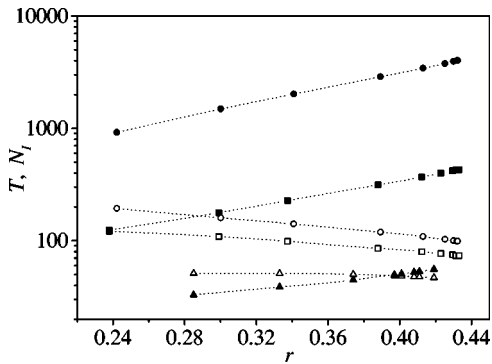

FIG. 6. Average values of the total evolution time T (empty symbols) and the maximum infected population N_I (full symbols) in the large-N_R regime as functions of the average fraction of final refractory individuals, $r = \langle N_R \rangle / N$, for networks with $K = 2$ and $N = 10^3$ (triangles), 10^4 (squares), and 10^5 (circles). Dashed lines have been drawn as a guide to the eye. In each data set, the leftmost and rightmost dots correspond to $p = 0.3$ and $p = 1$, respectively. From left to right, the randomness changes by steps of size $\delta p = 0.1$. For $N = 10^4$ and 10^5, the value $p = 0.35$ is also included. Each dot stands for an average over 10^3 realizations.

to in connection with Figs. 3 and 4, now for varying randomness. For fixed N, the final refractory population N_R grows with p. For the largest systems, in fact, N_R is practically doubled as p varies from 0.3 to 1. We thus verify again that propagation is more efficient for larger randomness. This effect is enhanced by the fact that, at the same time, the maximum infected population N_I increases and the total time T decreases. For large systems, T is reduced by a factor of 2 whereas N_I grows by a factor of 5, approximately. In summary, the process becomes simultaneously more effective and more rapid. Note, finally, the strong saturation in the values of r, T, and N_I as the randomness approaches its maximum $p = 1$.

Let us end this section by addressing the effects of changing the average number of neighbors per node, given by the parameter K. As for the localization-propagation transition, a growth in the number of neighbors implies that the critical randomness p_c decreases and that, for fixed p, the final fraction of refractory individuals increases [10]. These two results agree with the expected fact that propagation is more efficient for larger K. The same trend is observed in the parameters that characterize the evolution of the infected population: while the total time T decreases, the maximum number of infected individuals N_I grows. Our results for $K = 2$, in any case, are not qualitatively changed when other values of K are considered.

IV. PROPAGATION ON DYNAMIC SMALL WORLDS

Dynamic small worlds (DSWs) have been introduced as a variant to SWNs in the frame of a model for activity propagation in a system of mobile automata [15]. Instead of considering a frozen disordered interaction network, DSWs admit interactions between any two individuals occupying the nodes of a regular lattice. In the case of a one-dimensional array with periodic boundary conditions, at each interaction event, the partner of an infected individual is chosen with probability $1 - p$ among its $2K$ nearest neighbors, K clockwise and K counterclockwise. With the complementary probability p, the partner is chosen at random from the whole lattice. In this way, all the infected individuals have the chance to interact with arbitrarily distant partners, but the probability of distant interactions is controlled by the "randomness" p. Since, as in SWNs, an infected individual is chosen at each time step, real time must be updated according to Eq. (3).

The change from SWNs to DSWs, which conveys the replacement of frozen disorder by a stochastic process, is qualitatively similar to the introduction of the so-called annealed approximation in the study of disordered Boolean (Kauffman) networks [16]. A considerable advantage of DSWs over SWNs regards the numerical implementation, which does not require the generation of a new lattice at each realization—a highly time-consuming step in our specific system. However, the main virtue of DSWs—shared with the annealed model for Kauffman networks—is that, in principle, they admit a simpler analytical treatment. In particular, the limit $p = 1$ should be exactly described, in asymptotically large systems, by a mean-field-like approach.
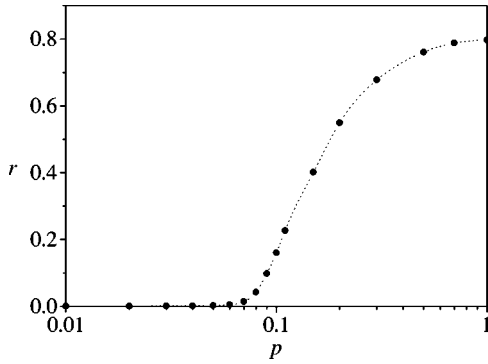
FIG. 7. Final fraction of refractory individuals, $r = \langle N_R \rangle / N$, as a function of the "randomness" p on a dynamic small world with total population $N = 10^4$ and $K = 2$. Each dot stands for an average over 10^4 realizations. The dashed line is a spline approximation, drawn as a guide to the eye.

We show in the following that the behavior of the rumor propagation model on a DSW bears remarkable similarity with the case of a SWN, though some significant quantitative differences are detected. Let us first of all point out that, as for the dependence of our model on the system size N and on the average number of neighbors per individual, $2K$, the features described in the preceding section for SWNs are qualitatively reproduced in DSWs. Consequently, we do not repeat the analysis for varying N and K, and focus here on the specific case $N = 10^4$, $K = 2$. The behavior for other values of N and K can be inferred from this case and the results for SWNs.

It has already been advanced [10] that our model on a DSW undergoes the same kind of localization-propagation transition found on SWNs. This is illustrated in Fig. 7, where we show the final fraction of refractory individuals $r = \langle N_R \rangle / N$ as a function of p, for $N = 10^4$ and $K = 2$. The critical point has considerably decreased, to $p_c \approx 0.06$. Meanwhile, as expected, the fraction r approaches the solution to Eq. (1), $r^* \approx 0.796$ as $p \to 1$. Note in fact that the original version of the model, discussed in Sec. II, is a kind of mean-field approximation of the small-world case, which becomes exact for $p = 1$.

As for SWNs, the nature of the localization-propagation transition in DSWs is revealed by the frequency distribution of the final number of refractory individuals, $f(N_R)$. Figure 8 shows this distribution for three values of p. For $p = 0.02$ we find a rapidly decaying function which, as in the subcritical regime on SWNs, results to be roughly exponential. In this case, in fact, the contribution of distant interactions is negligible, so that no significant differences are to be expected between DSWs and SWNs. For $p = 0.06$, which approximately corresponds to the critical point p_c in DSWs, the distribution is a power law over a substantial interval, $f(N_R) \sim N_R^{-\alpha}$. Remarkably, the exponent of this power law coincides—up to the numerical precision—with that obtained at the critical randomness in SWNs, $\alpha \approx 1.5$ (cf. Sec. II). Finally, above the critical point ($p = 0.1$), we find that the by now familiar bump structure at large N_R has developed. The strong similarity with the scenario on SWNs convinc-
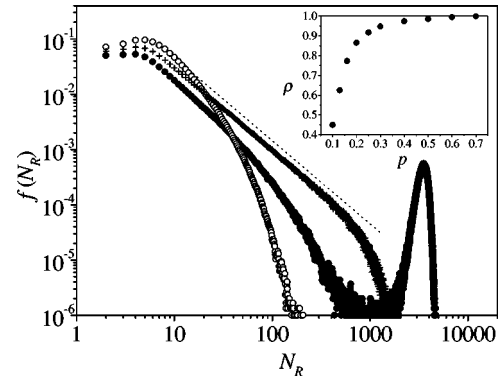

FIG. 8. Normalized frequency distribution $f(N_R)$ of the final number of refractory individuals N_R on a dynamic small world with a total population $N = 10^4$ and $K = 2$, for $p = 0.02$ (empty dots), $p = 0.06$ (crosses), and $p = 0.1$ (full dots). The frequency distribution was obtained from series of 10^6 realizations for each "randomness." The dashed straight line has a slope of -1.5. The inset shows the fraction ρ of realizations belonging to the large-N_R bump as a function of p, averaged over 10^3 realizations.

ingly suggests that the origin of the localization-propagation transition is the same for both systems.

The inset of Fig. 8 shows the fraction ρ of realizations that contribute to the bump, as a function of p. Comparing with Fig. 5, which shows the same results for SWNs, we note that—apart from the obvious consequences of the shift of p_c to the left—the fraction ρ attains considerably larger values. In particular, we find $\rho \approx 1$ for $0.6 \lesssim p$. For such values of p, therefore, the rumor propagates to distant regions and attains a finite portion of the system in virtually *all* realizations. An important contribution to this difference with SWNs is given by the following fact. In our SWNs, links between individuals are bidirectional. This implies that if an infected individual i transmits the rumor to a susceptible neighbor j, there is a relatively high probability that, in the future, the now infected individual j will (unsuccessfully) attempt to transmit the rumor to i and will become refractory. These unsuccessful trials for backward propagation are by far more improbable in DSWs, especially for large p, and the rumor spreading is consequently enhanced.

For $p < p_c$ the total evolution time T and the maximum number of infected individuals N_I satisfy the same power-law dependence of N_R as in SWNs. In fact, as far as long-range interactions remain infrequent, the evolution on SWNs and DSWs is essentially equivalent. The same argument can be extended for $p > p_c$ in small-N_R realizations. In this case, however, the exponent τ in the relation $T \sim N_R^\tau$ results to be smaller than for SWNs; now, we find $\tau \approx 0.57$. The moderate contribution of distant contacts is here enough to produce a considerable decrease of the total evolution time. Since contacts between any two individuals are now possible, propagation on DSWs is faster.

The fact that propagation on DSWs is faster and more effective than in SWNs becomes dramatically emphasized as soon as the large-N_R regime is analyzed. Figure 9 shows T and N_I as functions of N_R for large "randomness," ranging from $p = 0.5$ to 0.9. These plots show the "clouds" corre-
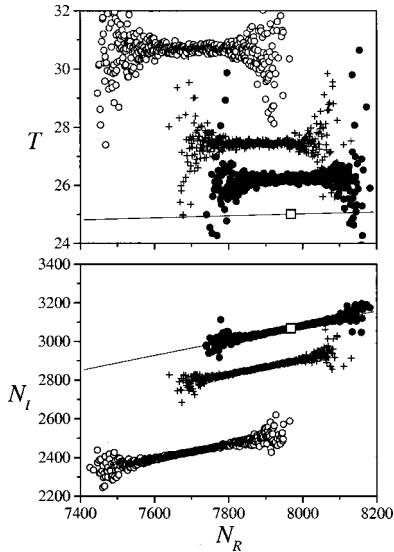
FIG. 9. (a) The total evolution time T and (b) the maximum number of infected individuals N_I, as functions of the final refractory population N_R, on a DSW with $N=10^4$ and $K=2$, for $p=0.5$ (empty dots), $p=0.7$ (crosses), and $p=0.9$ (full dots). Only the large-N_R region, corresponding to the bump structure, is shown. Data were extracted from 10^5 realizations for each value of p. In the cases where several values of T and N_I were obtained for the same value of N_R, they were averaged. Square symbols stand for the values of N_I and N_R, and the lower bound for T predicted by the mean-field approximation. The curves correspond to these same values for varying N.

sponding to the large-N_R bump structure, and are, therefore, analogous to the inserts of Figs. 3(b) and 4(b). The typical values of N_R, T, and N_I in these DSW realizations are to be compared with the corresponding values for SWNs, shown in Fig. 6. While, for $N=10^4$, the fraction $r=\langle N_R\rangle/N$ attains in SWNs a maximum average level of about 0.44 for $p=1$, in DSWs r reaches a typical value close to 0.8 for $p=0.9$. The differences in T and N_I are even more drastic. In SWNs, their extreme average values are $T\approx75$ and $N_I\approx440$, whereas in DSWs they change to $T\approx25$ and $N_I\approx3000$.

As the "randomness" of DSWs approaches its maximum value $p=1$, the system should be satisfactorily described by a mean-field approximation. The analytical treatment of our model within such approximation is developed in the Appendix. There we show that, for a given size N, it is possible to predict the values of N_I, N_R, and a lower bound for T. These values are compared with numerical results in Fig. 9. The agreement with the average of numerical results is very good for the largest "randomness," $p=0.9$. These results, however, show considerable fluctuations with respect to the values predicted by the mean-field approximation. Moreover, fluctuations in N_R, T, and N_I are closely correlated. Note that the same kind of correlations were suggested in SWNs by the results shown in the insets of Figs. 3(b) and 4(b). Since, as discussed above, DSWs can be more efficiently implemented in numerical experiments, our results in Fig. 9 correspond to a number of realizations considerably larger than for SWNs, and such correlations become apparent.

It turns out that the correlations between the values of T,

N_I, and N_R obtained in single realizations can be explained in terms of the mean-field approximation. In fact, calculating N_I and N_R, and the lower bound for T from this approximation for *different* values of the system size N—ranging from $N\approx9200$ to $10\,300$—we obtain the values shown in Fig. 9 as curves. These values successfully reproduce the correlation between the three quantities. Specifically, as N increases, T decreases slowly and N_R grows, while—as shown in the Appendix—N_I and N_R are linearly correlated. From a phenomenological viewpoint, these results can be interpreted as if in each individual realization the system appears to have an "effective" size—close to, but different from, its actual size—plausibly determined by variations in the effectiveness with which the rumor spreads over the population.

V. CONCLUSION

We have here studied the evolution of an epidemiclike model evolving on small-world geometries. The dynamics, which can be interpreted as the spreading of a rumor, is known to exhibit a transition between regimes of localization and propagation at a finite randomness of the underlying disordered geometry [10]. Epidemiological models on geometries that plausibly represent social networks and information webs—such as small-world and scale-free networks [17]—have recently attracted much attention, in view of their potential role in the description of actual risk situations associated with infectious diseases and computer viruses [9,18–21].

In our model, the effectiveness of propagation is characterized by the total number N_R of individuals that have been infected during the whole evolution. Generally, in a single realization of the process on an asymptotically large system of size N, propagation affects either a vanishingly small fraction of the population, $N_R/N\approx0$, or a finite fraction r. For a randomness p below the critical point p_c of the localization-propagation transition, only the small-N_R regime is observed, and the rumor remains localized within a limited neighborhood of its origin. For $p>p_c$, on the other hand, realizations in both regimes are observed. The fraction of realizations in the large-N_R regime, in fact, grows as the randomness increases.

The dynamics of our model is completely described by the evolution of the number n_I of infected individuals. A compact characterization of this evolution is given by the total time T elapsed up to the extinction of the infected population, the maximum number N_I of infected individuals at a given time, and the total number N_R of infected individuals during the whole evolution. The effectiveness of propagation increases when T decreases, because spreading is faster, and when N_R and N_I grow, because the rumor reaches a larger population.

Our results for small-world networks can be summarized as follows. For any value of p, the small-N_R regime is characterized by power-law correlations between T, N_R, and N_I. It has been suggested that these correlation could be explained in terms of a random-walk picture of the propagation process in the n_I space. A rigorous analogy, however, can only be achieved in terms of a biased random walk with a

rather complicated time-dependent bias. In the large-N_R regime, the values of T, N_R, and N_I obtained in single realizations are distributed around certain typical values, which vary as the network randomness p changes. Specifically, as p grows, T decreases and both N_R and N_I increase, indicating that the propagation process becomes increasingly effective. The three quantities show a quite marked saturation as the randomness approaches its limiting value $p=1$. The effectiveness of propagation is also improved, as expected, when the average number of neighbors per individual grows.

We have also studied these features in a so-called dynamic small world. Instead of considering a frozen network of interaction links, dynamic small worlds admit that distant contacts can occur between any two individuals, chosen at random at each evolution step. We have here shown that, as far as our model is concerned, propagation in a dynamic small world is qualitatively the same as on a small-world network. Namely, the same kind of correlations between T, N_R, and N_I and the same dependence with p observed on small-world networks are reproduced in dynamic small worlds. The main quantitative difference between both cases is that in dynamic small worlds the effectiveness of propagation is considerably higher. Evolution times are overall shorter and infected populations larger than on small-world networks. In qualitative terms, this is plausibly due to the fact that, in dynamic small worlds, the average number of interaction partners per individual is very large and the effect of backpropagation is comparatively negligible, especially, in large populations.

To our knowledge, this is the first time that the evolution of a dynamical process is compared in detail on small-world networks and in dynamic small worlds. It may be conjectured that our main conclusions regarding this comparison will hold for a large class of processes. A systematic comparison would in fact be desirable since, though small-world networks have attracted considerably more attention than dynamic small worlds, the latter have the advantage of easier analytical and numerical treatment and, moreover, provide a more realistic model of social systems with mobile individuals.

APPENDIX: MEAN-FIELD APPROXIMATION

A mean-field-like approximation for the model of rumor propagation described in Sec. II can be formulated assuming that each interaction event may occur with the same probability between any pair of individuals, i.e., neglecting the effects of spatial structure in the population. The frequency of such an event is, therefore, proportional to the product of the interacting populations. Denoting $n_S(t)$, $n_I(t)$, and $n_R(t)$, the susceptible, infected, and refractory populations, respectively, the mean-field evolution of our model is given by the equations

$$\dot{n}_S = -n_S \frac{n_I}{N}, \tag{A1}$$

$$\dot{n}_I = n_S \frac{n_I}{N} - n_I \frac{n_I+n_R}{N}, \tag{A2}$$

and

$$\dot{n}_R = n_I \frac{n_I+n_R}{N}. \tag{A3}$$

As expected, these equations imply that $n_S(t)+n_I(t)+n_R(t)=N$ is independent of time. Taking into account this conservation rule, the evolution equations can be implicitly solved in terms of the auxiliary variable

$$s = \int_0^t n_I(t')dt'. \tag{A4}$$

We point out that the introduction of the variable s in this continuous approximation is fully equivalent to the change from the real time scale to the measure of time in evolution steps used in the discrete model.

With the initial conditions $n_S(0)=N-1$, $n_I(0)=1$, and $n_R(0)=0$, the solutions to Eqs. (A1) to (A3) are

$$n_S(s) = (N-1)\exp(-s/N), \tag{A5}$$

$$n_I(s) = 1 - s + 2(N-1)[1 - \exp(-s/N)], \tag{A6}$$

and

$$n_R(s) = s - (N-1)[1 - \exp(-s/N)], \tag{A7}$$

respectively. From these solutions, some relevant quantities can be immediately calculated. The total number of steps S needed for the extinction of the infected population is the positive solution to $n_I=0$. This leads to the transcendental equation

$$S-1 = 2(N-1)[1 - \exp(-S/N)], \tag{A8}$$

which, for each value of N, can be accurately solved by numerical means. For asymptotically large N, it can be shown that $S=kN$, where $k\approx 1.594$ is the positive solution to $k=2[1-\exp(-k)]$ [note that $k=2r^*$; cf. Eq. (1)]. The final number of refractory individuals, N_R, can be evaluated from Eq. (A7) for $s=S$, i.e., at the end of the evolution. This yields

$$N_R = \frac{S+1}{2}. \tag{A9}$$

Actually, this result holds not only in the mean-field approximation, but for any value of p and N in both SWNs and DSWs, as discussed in the main text.

The step s_I at which the infected population $n_I(t)$ attains its maximum N_I is given by $\dot{n}_I=0$, i.e., $s_I=N\ln[2(N-1)/N]$. Replacing in Eq. (A6) we obtain the maximum number of infected individuals,

$$N_I = N - 1 - N \ln \frac{2(N-1)}{N} \approx (1 - \ln 2)N, \quad \text{(A10)}$$

where the right-hand side approximation holds for large N. In this limit, combination of the above results makes it possible to show that

$$N_I \approx \frac{2(1 - \ln 2)}{k} N_R \approx 0.385 N_R. \quad \text{(A11)}$$

The only problematic point in the comparison of the mean-field approximation with the original discrete model is

the evaluation of the total (real) time T elapsed up to the extinction of the infected population. As a matter of fact, in the mean-field approximation $n_I(t)$ decreases asymptotically and vanishes only for $t \to \infty$ (note that, however, this limit corresponds to a finite total number of steps S). The total time T must, therefore, result from a plausible definition using the mean-field results. In the main text we use the following criterion. We define T as the time needed for $n_I(t)$ to attain again its original value $n_I = 1$. In other words, T is the nontrivial solution to $n_I(t) = 1$, which can be accurately obtained from numerical integration of Eqs. (A1)–(A3). This gives a lower bound for the actual total evolution time, that can be directly compared with our numerical results.

[1] D.J. Watts and S.H. Strogatz, Nature (London) **393**, 440 (1998).
[2] M. Barthélémy and L.A.N. Amaral, Phys. Rev. Lett. **82**, 3180 (1999).
[3] M.E.J Newman and D.J. Watts, Phys. Lett. A **263**, 341 (1999).
[4] M.E.J. Newman, C. Moore, and D.J. Watts, Phys. Rev. Lett. **84**, 3201 (2000).
[5] A. Barrat and M. Weigt, Eur. Phys. J. B **13**, 547 (2000).
[6] D.J. Watts, *Small Worlds* (Princeton University Press, Princeton, 1999).
[7] C.F. Moukarzel, Phys. Rev. E **60**, R6263 (1999).
[8] M. Argollo de Menezes, C.F. Moukarzel, and T.J.P. Penna, Europhys. Lett. **50**, 574 (2000).
[9] M. Kuperman and G. Abramson, Phys. Rev. Lett. **86**, 2909 (2001).
[10] D.H. Zanette, Phys. Rev. E **64**, R050901 (2001).
[11] J.D. Murray, *Mathematical Biology*, 2nd ed. (Springer, Berlin,

1993).
[12] J.C. Frauenthal, *Mathematical Modelling in Epidemiology* (Springer, Berlin, 1980).
[13] A. Sudbury, J. Appl. Probab. **22**, 443 (1985).
[14] E.W. Montroll and B.C. West, in *Fluctuation Phenomena*, edited by E.W. Montroll and J.L. Lebowitz (Elsevier, Amsterdam, 1979).
[15] S.C. Manrubia, J. Delgado, and B. Luque, Europhys. Lett. **53**, 693 (2001).
[16] B. Derrida and Y. Pomeau, Europhys. Lett. **1**, 45 (1986).
[17] A.L. Barabási and R. Albert, Science **286**, 509 (1999).
[18] M.E.J. Newman and D.J. Watts, Phys. Rev. E **60**, 7332 (1999).
[19] C. Moore and M.E.J. Newman, Phys. Rev. E **61**, 5678 (2000).
[20] R. Pastor-Satorras and A. Vespignani, Phys. Rev. Lett. **86**, 3200 (2001).
[21] R. Pastor-Satorras and A. Vespignani, Phys. Rev. E **63**, 066117 (2001).